ARTICLES

Time-Series Analysis of Large Igneous Provinces: 3500 Ma to Present

Andreas Prokoph, Richard E. Ernst,[1] *and Kenneth L. Buchan*[2]

Speedstat, 36 Corley Private, Ottawa, Ontario K1V 8T7, Canada
(e-mail: aprokocon@aol.com)

ABSTRACT

We outline an efficient integrated wavelet, a spectral, and a cross-spectral approach for the time-series analysis of geologic data. Here these techniques are applied to a database of 154 large igneous provinces (LIPs) in order to test for cycles, trends, and abrupt changes in temporal distribution since 3500 Ma. The average frequency of events is relatively constant and supports an overall model of semicontinuous temporal emplacement of LIPs. However, several weak cycles were obtained in the analysis. Those of longest duration are a ~170-m.yr. cycle from 1600 Ma to present and in the late Archean, a ~330-m.yr. cycle from about 3000 to 1000 Ma, a cycle decreasing in length from 730 to 550 m.yr. over the interval 3500 Ma to present, and a still weaker cycle increasing from 900 to 1000 m.yr. over the interval 2000 Ma to present. Additional cycles of shorter duration include a ~250-m.yr. cycle in the late Archean, a ~230-m.yr. cycle in the Phanerozoic, a ~105-m.yr. cycle in the early Proterozoic, and several <60-m.yr. cycles occurring in scattered intervals. The uncertainties in the cycle patterns preclude a simple correlation with previously interpreted forcing functions: a ~30-m.yr. cometary impact, a 270-m.yr. galactic year, a 500–300-m.yr. supercontinent cycle, and a ~800-m.yr. resonance between tidal and free oscillations of the core. However, our ~170-m.yr. interval spacing is associated with clusters of LIP events over the past 1500 Ma. Future time-series analyses on improved versions of the LIP database (and appropriate subsets) will be required to test the robustness of the cycles we observe and to identify underlying forcing functions.

Online enhancement: table.

Introduction

Large-volume, short-duration, mainly mafic magmatic events that are not associated with normal plate boundary processes are termed large igneous provinces (LIPs; e.g., Coffin and Eldholm 1994, 2001; Ernst and Buchan 2002). On continents, such LIPs are termed continental flood basalts, and in oceanic areas, they are called oceanic plateaus or ocean basin flood basalts depending on resulting topography (Coffin and Eldholm 2001). Continental flood basalts can be as large as several million cubic kilometers (e.g., Siberian Traps; Reichow et al. 2002), whereas the largest oceanic plateau, Ontong Java, has a volume of 44.4 million cubic kilometers (Coffin and Eldholm 2001). The duration of the main stage of LIP emplacement is typically <10 m.yr. and often as short as 1 m.yr., with continued activity at a generally reduced level. Many LIPs are thought to be generated from a rising mantle plume that originates from a thermal boundary layer either at the base of the mantle or at a midmantle boundary (e.g., Campbell 2001). On reaching the base of the lithosphere, an ascending plume causes domal uplift and triple junction rifting and may be associated with continental breakup (e.g., Condie 2001; Ernst and Buchan 2001*b*). In addition, and most importantly in the context of this article, the plume head partially melts to form an LIP. Other models for the origin of LIPs include rift-related decompression melting (e.g., White and McKenzie 1989) and convection between adjacent thick and

Manuscript received December 3, 2002; accepted July 14, 2003.

[1] Author for correspondence: Magnetic Research Facility for Tectonic Studies (GCS campus), Geological Survey of Canada, 601 Booth Street, Ottawa, Ontario K1A 0E8, Canada; e-mail: rernst@nrcan.gc.ca.

[2] Magnetic Research Facility for Tectonic Studies (GCS campus), Geological Survey of Canada, 601 Booth Street, Ottawa, Ontario K1A 0E8, Canada.

[The Journal of Geology, 2004, volume 112, p. 1–22]

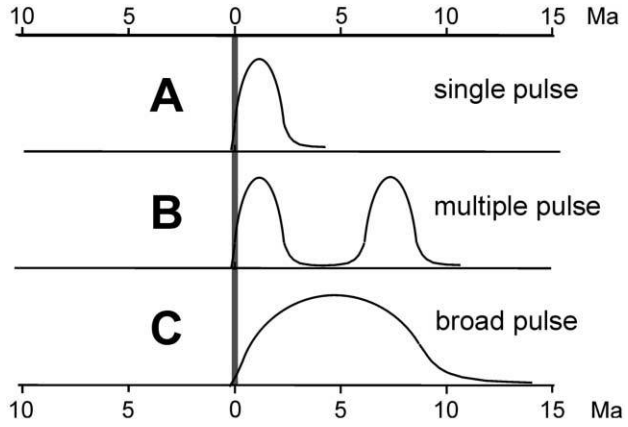

Figure 1. Schematic models of volume versus time for different types of large igneous provinces (LIP) events with our pick of the event starting age (time "0"). *A*, Single event of short duration followed by a minor activity continuing to younger age (interpreted as plume head event followed by plume tail activity). *B*, Multiple pulses of LIPs. *C*, LIP with broad age range.

thin lithospheric domains (e.g., King and Anderson 1998).

The volcanic portion of older continental LIPs is lost to erosion and deformation, and oceanic LIPs are largely destroyed during ocean closure (e.g., Coffin and Eldholm 2001). However, in the Paleozoic and Proterozoic, continental LIPs can be reliably recognized by their plumbing system (which consists of giant dike swarms, sill provinces, and large layered intrusions) and by the erosional remnants of flood basalts (Ernst and Buchan 2001*a*). The oceanic LIP record may be recognized in some accreted volcanic packages and ophiolite complexes (e.g., Coffin and Eldholm 2001; Moores 2002; Ernst and Buchan 2003).

The extrapolation of the LIP record into the Archean is more speculative. There are erosional remnants of relatively flat-lying, "normal" flood basalts, such as the Fortescue sequence of the Pilbara Craton of Australia and the Ventersdorp sequence of the Kaapvaal craton of southern Africa (Eriksson et al. 2002). However, Archean mafic magmatism is usually in the form of greenstone belts, which comprise variably deformed and metamorphosed sequences, typically fragmented into fault-bounded packages (assemblages). Even though it is possible on a local scale to recognize short-duration events of significant (multikilometer) stratigraphic thickness, it is hard to correlate between packages. Recent advances have been made in some greenstone belts in tracking komatiite-bearing tholeiitic sequences over LIP-scale areas (e.g., Bleeker 2002).

There have been numerous attempts to identify cycles and trends in the spectrum of LIPs through time. For instance, Yale and Carpenter (1998) used the dike swarm database of Ernst et al. (1996) to infer a link with a supercontinent cycle of 300–500 m.yr. Integrating the Mesozoic-Cenozoic record of flood basalts with other data sets, Rampino and Caldeira (1993) recognized 26-, 23-, and 15-m.yr. cycles that they linked to periodic impact of comets. Larson (1991, 1997) recognized unusually high oceanic LIP activity and associated accelerated ridge spreading at 120–80 Ma. Such periods of enhanced and widely distributed LIP activity may be representative of a class of multiple plume events (sometimes termed superplume events) occurring intermittently throughout Earth's history (Condie 2001; Ernst and Buchan 2002; Ernst et al. 2003) and may be potentially linked to periods of peak production of oceanic crust (Condie 2001) or supercontinent breakup (Storey 1995; Li et al. 2003). Detailed analyses of portions of the LIP record have been carried out by Isley and Abbott (1999, 2002). Their 1999 article focused on comparing the LIP record with the timing of iron formations prior to 1.5 Ga. Their 2002 article focused on a spectral analysis of high Mg magmas (representing a strong LIP proxy) and revealed the most significant cycles of $819 + 204/-137$ m.yr. and 273 ± 20 m.yr. and the less significant cycles of 315 ± 25 m.yr. and 372 ± 35 m.yr. (see peak values in fig. 1; exact values for the mean and 1σ uncertainties provided by A. Isley, pers. comm.). In addition, they recognized cycles of 26 ± 3 and 34.5 ± 4.5 (1σ) m.yr. during analysis of shorter time intervals (256 m.yr. long) in the Archean and Phanerozoic, respectively. The long period (~800-m.yr.) cycle was linked to resonance between free-core and forced-core nutations. The proposed 273-m.yr. cycle was linked to a galactic year cycle and the 26–35-m.yr. cycle to periodic cometary impacts.

The validity of observed cycles is critically dependent on the robustness of the LIP database (Ernst et al. 2003). Our purpose in this article is to perform a time-series analysis on the most recent comprehensive LIP database (table 1, available in the electronic edition of the *Journal of Geology* and also available from the *Journal*'s Data Depository in the *Journal of Geology* office upon request, based on Ernst and Buchan 2001*a*) to identify patterns and to compare our results with the time-series analyses of previous workers.

Preliminary analyses of the LIP record (Ernst and Buchan 2001*a*, 2002) indicated that the record is

relatively continuous. A few significant gaps are observed, but it is not clear whether these are real or merely artifacts of an incomplete database. Estimates of average plume frequency based on this record indicate an average frequency of one plume every 20 million years since the Archean (Ernst and Buchan 2002), and for the more completely preserved oceanic plus continental record of the past 250 m.yr., an estimate of one per 10 m.yr. (Coffin and Eldholm 2001).

Our analysis of the Ernst and Buchan (2001*a*) LIP database utilizes a more sophisticated analysis to search for patterns in the temporal distribution of events than previously applied. The analyses of Isley and Abbott (2002) used spectral analysis, Yale and Carpenter (1998) used slopes on cumulative percentage diagrams weighted by inferred LIP volumes, and Rampino and Caldeira (1993) used moving window analysis/Gaussian filtering/Fourier analysis. This article combines wavelet, spectral, and cross-spectral techniques (Prokoph and Barthelmes 1996; Prokoph and Veizer 1999) to analyze the LIP data for the last 3.5 Ga. We assess the following: (1) completeness of the LIP record; (2) presence of cycles, trends, and abrupt changes in the LIP distribution pattern through time; (3) consistency of cycles and trends for several subsets of the LIP database; and (4) significance of cycles in the record and possible links with various Earth system cycles.

Database Used for Time-Series Analysis

Selection of LIPs for Analysis. The LIP database used in this article is that of Ernst and Buchan (2001*a*), with minor updates, and is presented in table 1.

The characteristics of the Ernst and Buchan (2001*a*) database are summarized below. After a systematic literature search, and partly building on earlier compilations (Coffin and Eldholm 1994 for young LIPs; Tomlinson and Condie 2001 for Archean LIPs; and Isley and Abbott 1999 for units older than 1.5 Ga), Ernst and Buchan (2001*a*, 2002) assembled a LIP database covering the entire geological record and used it to assess the distribution of plume head magmatic events in space and time back to 3.8 Ga. A total of 304 possible events were identified and divided into three classes, "A," "B," and "C," according to the likelihood of their being related to an arriving mantle plume head. Thirty-five of the mafic magmatic events were confidently related to the arrival of a mantle plume head and were rated A on the basis of the following criteria: emplacement of a large amount (areal extent of >100,000 km^2) of magma in a short time (a few million years), the presence of a giant (≥ 300 km radius) radiating dike swarm, or a link to a present-day hot spot. Using other criteria including the identification of "plume" geochemistry, the presence of high Mg magmas (picrites and komatiites), event size, duration (areal extent >100,000 km^2 and emplaced within uncertain age range or >20,000 km^2 emplaced within a few million years), and/or the presence of giant (≥ 300-km-long) linear dike swarms, an additional 197 events were rated B. The remaining 76 events, the majority of which are rift related, require further study to assess a plume head (and LIP) connection and were rated C.

For this study we utilize a slightly updated version of this LIP database and select only events that have a 2σ-age uncertainty ≤ 50 m.yr. and that are also rated (according to the above criteria) as A or B. Events with a C rating were not included in the present time-series analysis. Table 1 includes 35 events rated A and 173 rated B.

Selection of LIP Initiation Age. For the time-series analysis, a single age and uncertainty must be selected for each LIP. This selection is not straightforward, because some events are more protracted than others, some exhibit multiple pulses, and some exhibit a range of ages that could reflect either multiple pulses or a continuous age range (fig. 1). To add to the complexity, in many cases the number of age determinations on a single event is small, and so the spectrum of ages for each event is impossible to assess.

The strategy in this article is to estimate the age of onset of the first pulse of the LIP rather than its peak or any subsequent pulse. For LIPs that are generated by mantle plumes, the onset of the first pulse dates the arrival of a mantle plume head. A subsequent pulse may represent a later upwelling along the same plume stalk or be related to rifting that enhanced asthenospheric partial melting. In cases where only one precise age was available for an event, we provisionally choose this age as the LIP initiation age. Where multiple precise ages were available, we choose the oldest age.

The various patterns of LIP magmatism (fig. 1) are further described with examples. Many events exhibit a burst of magmatism followed by a tail-off of activity over a period of 10 m.yr. or more (fig. 1*A*). In the Columbia River Province, 95% of the volcanism occurred within about 2 m.yr., but activity continued at a very decreased level for another 15 m.yr. to the present (fig. 5 in Tolan et al. 1989). Similarly, the main phase of Siberian Trap volcanism lasted about 1 m.yr., with most of the magmatism occurring in less than 5 m.yr. (Ni-

kishin et al. 2002). In the case of the Deccan Traps the burst of activity lasted less than 1 m.yr. (Courtillot et al. 1999).

Many LIPs seem to involve multiple pulses of magmatism (fig. 1*B*). The North Atlantic Igneous Province consists of an initiation pulse at 62 Ma and a successive (rift-related) pulse at 56 Ma (Saunders et al. 1997). The Kerguelen oceanic plateau includes two pulses of short duration at 118 and 100 Ma (Coffin et al. 2002; Duncan 2002). Most of the Paraná-Etendeka LIP of South America and western Africa is dated at about 132 Ma, but there is a significant pulse at 138–135 Ma (Peate 1997). A classic example of a multiple pulse event is the Keweenawan event of the Midcontinent Rift of North America where an initial burst of activity occurred at 1110 Ma, but an equally significant pulse occurs at 1100 Ma (event 90 in Ernst and Buchan 2001*a*).

Another possible example of a multiple pulse event is the protracted Matachewan event with ages of ca. 2490, 2475, and 2446 Ma, represented by dike swarms, layered intrusions, and volcanic rocks (event 206 in Ernst and Buchan 2001*a*). However, the number of dates available at present are too few to rule out the possibility of a continuum of activity (fig. 1*C*).

Methodology of Time-Series Analysis

Data Preprocessing: Producing Gaussian Probability Functions. All data sets (containing age and uncertainty values for each event) have been transformed to equidistant (1-Ma age interval) time series by using the Gaussian probability function to determine the probability (0–1) of each event occurring in a specific 1-Ma time interval according to its mean age and age uncertainty. Two approaches can be used for summing the probabilities related to each event. Isley and Abbott (1999, 2002) used the probabilistic "AND" where the final time series was produced as the sum of many smooth, bell-shaped curves, each one representing one age and its corresponding error.

In contrast, we employ the probabilistic "OR." The larger of the two overlapping values is applied to the age interval (OR), not the sum of both values (AND), because we wish to determine the probability of any LIP event occurring at this age, not the numbers of events occurring at a given time. While the latter would be worth a separate analysis, this is impractical at present given our poor understanding of Precambrian continental reconstructions, which prevents assessment of whether same-aged LIPs found on different cratonic blocks represent a fragmented single LIP or multiple LIPs (Ernst and Buchan 2002). A number of analytical techniques were applied to the data.

Wavelet Analysis. The continuous wavelet transform of a time series $f(t)$ is defined as

$$W_{\psi(a,\,b)} = \left(\frac{1}{\sqrt{a}}\right)\int f(t)\psi\left(\frac{t-b}{a}\right)dt, \qquad (1)$$

where ψ is the base wavelet (which is here the Morlet wavelet) with a length that is usually much shorter than the time series $f(t)$. The continuous wavelet transform allows detection of nonstationarities and periodicities in a similar way as advanced evolutionary spectral analysis (e.g., multiple taper spectral analysis; Park and Maasch 1993).

For this project, $\sqrt{a}$ is replaced by a, the so-called L1 norm (Prokoph and Barthelmes 1996), which calculates the wavelet coefficients W, comparable to the power in spectral analysis (i.e., variance). The variable a is the scale factor that determines the frequencies (or wavelengths). The variable b is the shift of the analysis window in time, so that varying b represents the sliding window of the wavelet over $f(t)$ (Chao and Naito 1995). The Morlet mother wavelet (shifted and scaled) is defined as

$$\psi^{l}_{a,\,b}(t) = \pi^{-1/4}(al)^{-1/2}e^{-i2\pi(1/a)(t-b)}e^{-(1/2)[(t-b)/al]^2}. \qquad (2)$$

The parameter l represents the relation between periodicity and depth resolution. Parameter $l = 10$ was chosen, which gives sufficiently precise results in the resolution of depth and frequency, respectively.

In our algorithm, the trendline is removed, and the mean value of $x(t)$ is standardized to 0. The visualizing of $W(a, b)$ has been carried out by interpolation and coding with appropriate shades of gray. The three most significant (major) periodicities $a_{w\max_{1-3}(b)}$ through the whole time series can be used to identify variations in LIP event rate directly from the wavelet coefficients. The three most intense wavelengths are determined as follows: after the peak value is identified, the second most intense wavelength must be more than 5% shorter than the first, and the third must be at least another 5% shorter than the second. This approach respects bandwidth uncertainties.

Spectral Analysis (Fourier Transform). Spectral analysis is defined by

$$P_f^2 = \int x(t)e^{i2\pi ft}dt, \qquad (3)$$

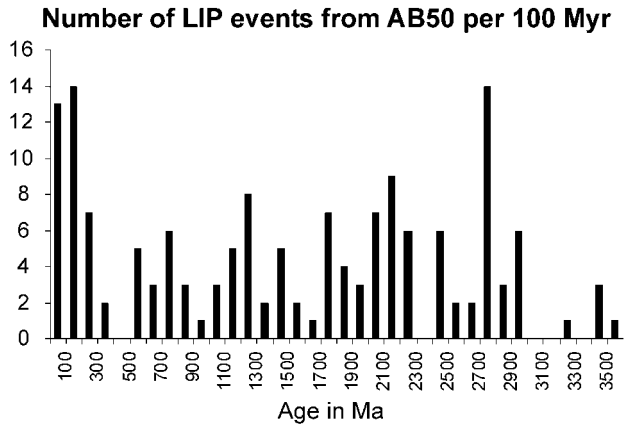

Figure 2. Histogram of distribution of large igneous provinces (LIP) events (mean ages) through time in 100 Ma bin intervals. Note that there is no trend in the distribution that would indicate effects of crust recycling (Veizer 1988) on the preservation of LIP events.

with $x(t)$ as the discrete time series, f the frequency (i.e., $1/a$), and P as spectral power (Davis 1986).

The wavelet approach contrasts with the Fourier analysis. The Fourier analysis is not able to detect temporal discontinuities, is incapable of distinguishing between continuous low-amplitude and nonstationary high-amplitude signals, and is not able to yield information on the temporal persistence of periodicities. The relative mean values of the wavelet coefficients and the spectral (Fourier) power are also slightly different, because of the standardization of the wavelet coefficients (mean = 0, trend line removed).

Data Processing Errors. Of importance for this project is the transform of cyclic signals from time domain (stratigraphic position) to frequency (or cycle length) domain. According to the Fourier transform, every signal in a time series can be described as

$$x(t) = a \sin(2\pi f + \varepsilon_p) + \varepsilon_r, \tag{4}$$

with ε_r as random error (or "white" noise) and ε_p as phase error, a long memory error also called red noise. Random (white noise) errors ε_r affect all frequencies in the same amplitude and form a background noise with small peaks in power spectra up to

$$P_f = Pw_f = \frac{2\sigma^2}{N}, \tag{5}$$

with σ^2 as variance of the whole data set (e.g., Davis 1986).

The "red" noise Pr_f describes the long-term memory, such as long tends and cycles with wavelength $1/f > \Delta tN$, and can be calculated from

$$Pr_f = Pw_f \frac{1 - p^2}{1 - 2p \cos \pi(f/f_N) + p^2}, \tag{6}$$

with p as the lag-one autocorrelation coefficient, under the assumption that autocorrelation decays exponentially as a function of time (Mann and Lees 1996).

Confidence levels are commonly calculated from the probability that an event belongs to a normal (random) distribution or does not (e.g., Davis 1986). However, the signals cannot be completely randomly distributed, because by using the Gaussian probability function for age-uncertainty filtering, nearby signals became lag-one autocorrelated. Thus, we determine the confidence levels to be independent of frequency distribution by calculating the power from the original signals randomly shuffled. The 10% highest power value of the shuffled data gives the 90% confidence interval (Rn_{90}) for the original data, the 5% highest power value gives the 95% confidence interval (Rn_{95}), and the 1% highest power value of the shuffled data gives the 99% confidence interval (Rn_{99}), respectively. Then, we replace the white noise parameter Pw_f in equation (6) by Rn_{90}, Rn_{95}, and Rn_{99} and provide an estimate for lag-one autocorrelation (red noise) under consideration of distribution-independent confidence levels.

Data Subgroups. The following subsets of data are utilized in this analysis, and the data are listed in table 1. Ratings A and B reflect designations for individual LIPs as discussed in "Selection of LIPs for Analysis."

(1) AB50 ($n = 154$) events are those rated A or B with an age uncertainty ($\pm 2\sigma$) less than or equal to 50 m.yr., (2) AB10 ($n = 120$) events are those rated A or B with an age uncertainty ($\pm 2\sigma$) less than or equal to 10 m.yr., (3) A10 ($n = 35$) events are those rated A with an age uncertainty ($\pm 2\sigma$) less than or equal to 10 m.yr., (4) B10 ($n = 86$) events are those rated B with an age uncertainty ($\pm 2\sigma$) less than or equal to 10 m.yr., (5) AB50-continental ($n = 115$) events were emplaced on continental crust and are rated A or B with an age uncertainty ($\pm 2\sigma$) less than or equal to 50 m.yr., and (6) AB50-oceanic ($n = 32$) events were emplaced on oceanic crust and are rated A or B with an age uncertainty ($\pm 2\sigma$) less than or equal to 50 m.yr.

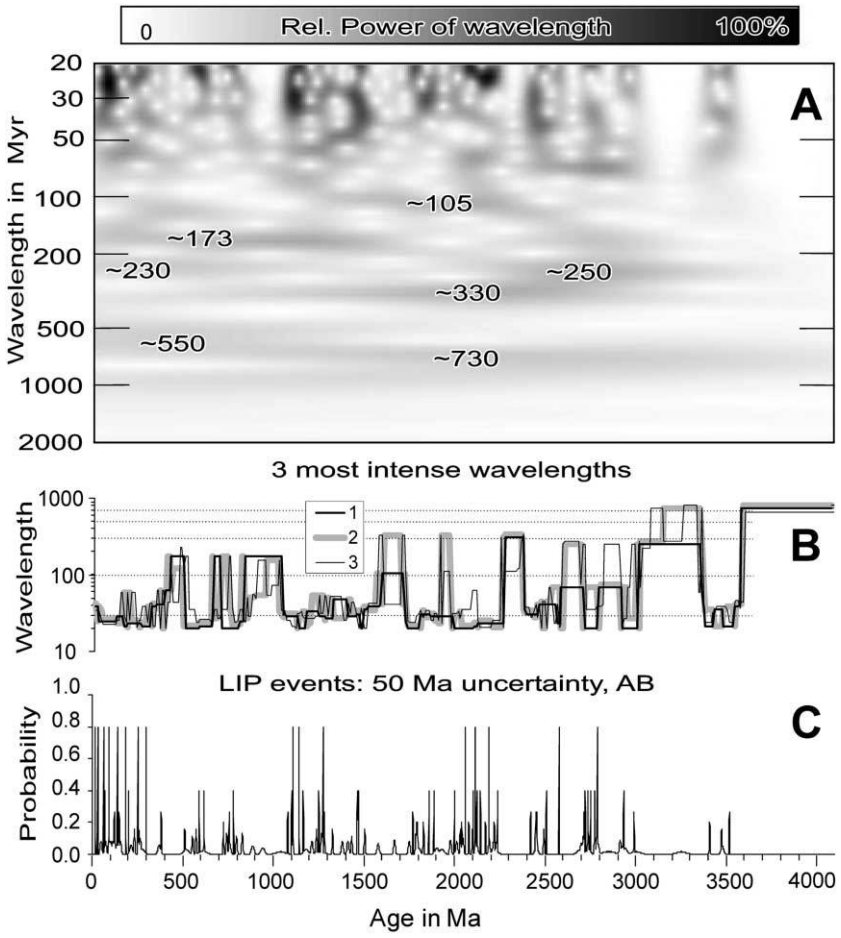

Figure 3. Wavelet analysis of AB50 data (154 events). Data described in text and listed in table 1. *A*, Wavelet scalogram, with continuous gray shading. *B*, Three most significant periodicities. *C*, Gaussian distribution of data. The three most intense wavelengths are determined as follows: after the peak value is identified, the second most intense wavelength must be more than 5% shorter than the first, and the third must be at least another 5% shorter than the second. This approach respects bandwidth uncertainties.

Results

Data Completeness. One of the major concerns relates to the completeness of the LIP event data set, in particular whether with increasing age, increasing numbers of LIPs are lost due to crustal recycling processes (see crustal recycling models in Veizer 1988). The overall distribution of AB50 events of the last 3500 Ma is relatively constant except for peaks in the intervals 200–0 Ma and 2800–2700 Ma (fig. 2). Thus, if recycling had occurred, then the rate of LIP production would need to have been systematically higher in the past to compensate for ongoing recycling losses. A simpler interpretation is that the crust recycling/erosion process (Veizer 1988) does not significantly affect the preservation of LIPs, probably because the deeper, noneroded parts of the crust still preserve the "roots" (e.g., dike swarms) of eroded surface features (e.g., flood basalts), even for the oldest LIPs. The relatively even distribution of events through the last 3500 Ma and the good precision of their dating suggest that this data set (table 1) is a robust record of Earth's LIP history.

Wavelet Analysis of the Full Data Set AB50. Before wavelet analysis, the data set is converted to a smooth curve by computing a Gaussian distribution for each event based on age and uncertainty and then superimposing the events using the OR criteria (discussed earlier). In each of figures 3–10, we provide a scalogram calculated from equation (1) (*A*), a graph of the top three cycles (wavelengths; *B*), and the smoothed curve of the original data (*C*), all plotted against age. Note that we label cycles with their average peak value, although in many

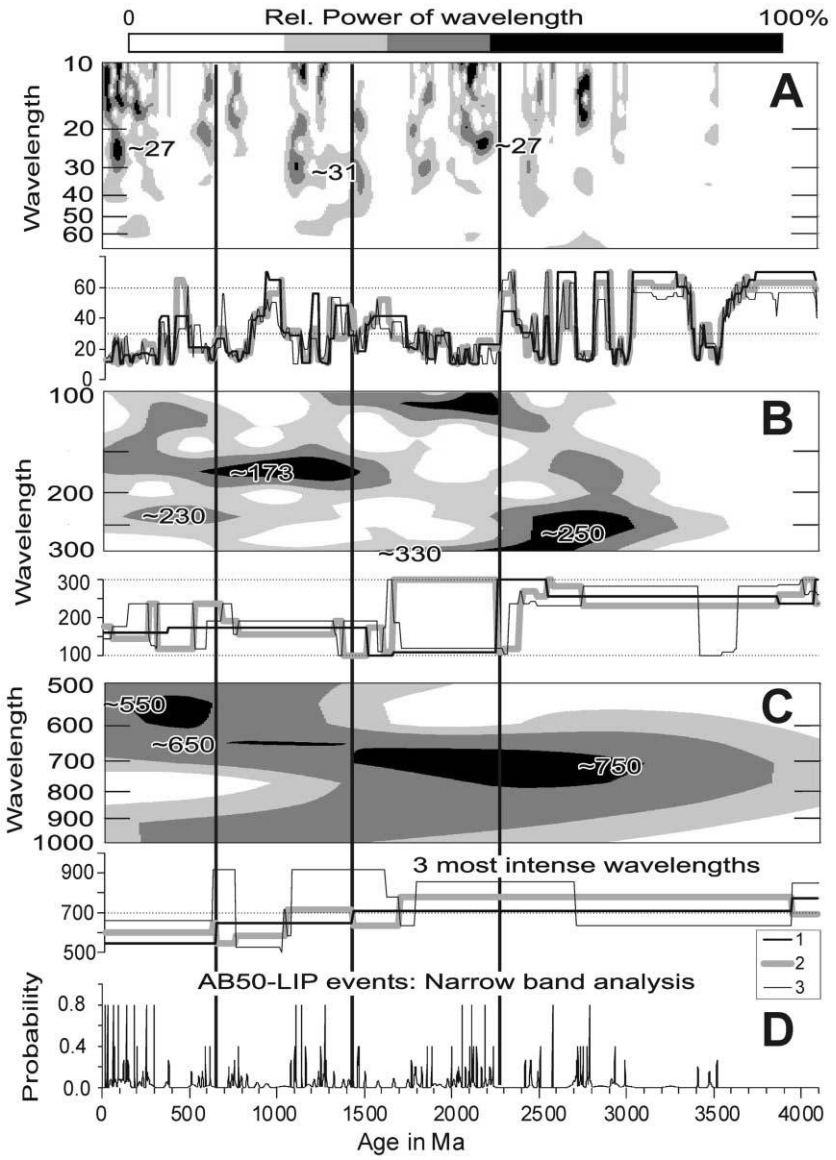

Figure 4. Narrow band wavelet analysis using AB50 data (154 events). Data described in text and listed in table 1. *A*, 10–70-m.yr. bandwidth. *B*, 100–300-m.yr. bandwidth. *C*, 500–1000-m.yr. bandwidth. The vertical lines mark distinct changes in the cycle pattern ~650 Ma, ~1450 Ma, and ~2300 Ma. Note the episodic, nonpersistent occurrence of 27–31-m.yr. cyclicity.

cases the cycle is represented by a broad band rather than a sharp peak. The peak value represents the most significant cycle length at a given time interval. The broad widening of the wavelet coefficient band is a result of the bandwidth uncertainty (~7% of wavelength) and possible gradual shifts in cycle length. The wavelet method applied to the AB50 data set (figs. 3, 4) provides a starting point for our analysis. The AB50 represents the entire data set of table 1, data rated A and B with a 2σ-age uncertainty of ≤ 50 m.yr. In subsequent sections, we examine the robustness of the analysis based on the full AB50 data set by redoing the analysis using selected subsets of the database (subsets 2–6 above; figs. 5–10).

The AB50 data set was studied using both broadband (fig. 3) and narrowband analyses (fig. 4). Overall, there are no cycles that have both high intensity and persist throughout the entire age range, suggesting that the first-order pattern is semirandom. However, the spectra do exhibit weak cycles that are summarized in table 2. A very weak ca. 1000–

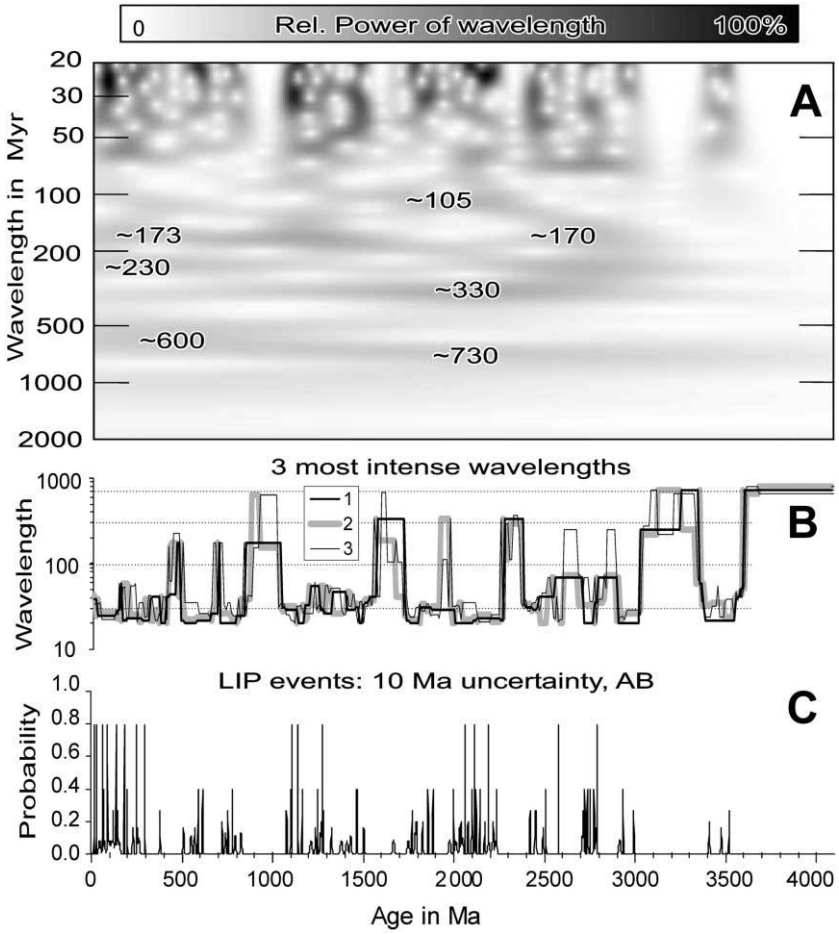

Figure 5. Wavelet analysis of AB10 data (120 events). Data described in text and listed in table 1. *A*, Wavelet scalogram. *B*, Three most significant periodicities. *C*, Gaussian distribution of data. Note that the long wavelengths (>100 m.yr.) are less significant than in the 50-m.yr. uncertainty data (AB50), but the high-resolution cycles are more intense and persistent. For example, the 25–30 Ma band is represented by episodic occurrence of cycles.

900-m.yr. cycle is present from about 2000 to 0 Ma. Of greater significance is a persistent but weak cycle that decreases from 730 to 550 m.yr. over the interval 3500 Ma to the present. The present data set is not sufficiently robust to rule out a stepwise change from 730 to 650 to 550 Ma or overlapping changes in cycle length. A 330-m.yr. cycle is observed from 3000 to 1000 Ma. A 250-m.yr. cycle persists from 3300–2100 Ma, and a similar and possibly related cycle of 230 m.yr. occurs from 700 Ma to the present. A 170-m.yr. cycle occurs in the late Archean and from 1600 Ma to the present. A 105-m.yr. cycle is noted from 2200 Ma to 1400 Ma.

Analysis of the <100-m.yr. wavelength band of AB50 indicates an absence of cycles between about 100 and 70 m.yr. (fig. 3). However, there is a complicated pattern of short-duration cycles less than 60 m.yr., with perhaps the most significant at about 27–31 and at 15–10 m.yr. However, although locally intense, these <60-m.yr. cycles have poor persistence probably because few intervals have enough data to resolve high-frequency cycles (cf. fig. 3*B*, 3*C*). Furthermore, the shortest wavelength cycle (15–10 m.yr.) is close to the resolution of the data and may be a statistical artifact.

Wavelet Analysis of Data Subsets. Several subsets of the full AB50 data set were analyzed in order to assess the robustness of the cycles obtained from the full data set and to help identify the controls on the observed cycles. One subset AB10 contains only the highest resolution data (i.e., the data with 2σ-age uncertainties ≤ 10 m.yr.; fig. 5). A further AB10 analysis was focussed on the LIPs of the past 300 m.yr. in order to assess the high-frequency patterns in this age range (fig. 6), which contains the best-preserved portion of the data set.

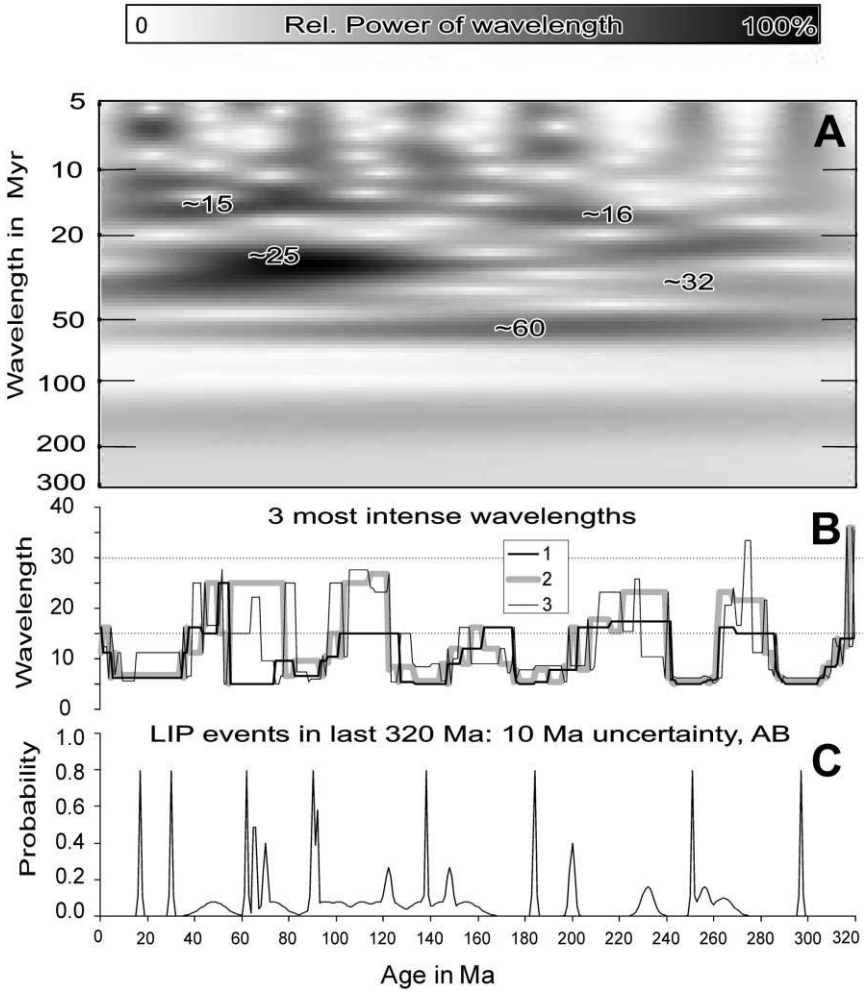

Figure 6. Wavelet analysis of AB10 data during last 320 Ma. Data described in text and listed in table 1. *A*, Wavelet scalogram. *B*, Three most significant periodicities. *C*, Gaussian distribution of data. Note that the 25–32-m.yr. period band is nonpersistent in the record, but a 15–16-m.yr. band appears stronger.

The LIP database was also separated into oceanic and continental events (figs. 7, 8) in order to test whether the type of crust influences the timing of LIPs. This analysis is most robust for the young (300 m.yr.) record where the assignment of continental and oceanic LIPs is reliable. The analysis is least conclusive in the Archean where the setting of LIP-type greenstone belts is less certain (e.g., Bleeker 2002). Finally, the effect of LIP classification was investigated by separately studying LIPs rated A (fig. 9) and B (fig. 10). As indicated in an earlier section, an A rating indicates a reliable link with a mantle plume, while a B rating indicates a probable link with a mantle plume. The subset analyses are summarized below with respect to the cycle lengths identified in the full AB50 analysis. A weak 1000–900 m.yr. cycle is present in subsets AB10 or AB50-oceanic (figs. 5, 8) but not in AB50-continental, A10, and B10 (figs. 9, 10).

A 730–550-m.yr. cycle is observed in all data subsets except the A10 (fig. 9). Between 700 Ma and the present, A10 data (fig. 9) exhibit a 520-m.yr. cycle, which is only slightly shorter than the 730–550-m.yr. cycle of the full AB50 data set. The restriction of this cycle to the young portion of A10 probably reflects the fact that most of the A10 data is less than 800 Ma in age. Since the B10 data (fig. 10) does show the cycle throughout, although more weakly in the last few hundred m.yr., it might be interpreted that A and B represent complementary data sets. This cycle is also present in the AB50-continental data and is weakly present as a 650-m.yr. cycle in the sparse AB50-oceanic data (figs. 7, 8).

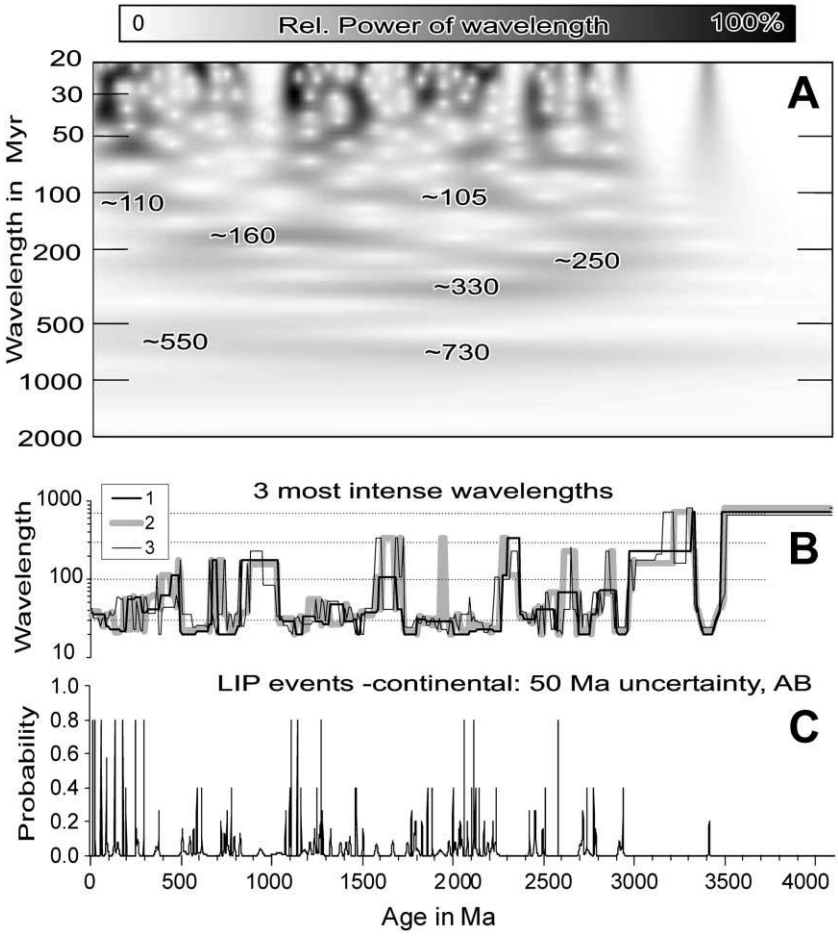

Figure 7. Wavelet analysis of AB50-continental data (115 events). Data described in text and listed in table 1. *A*, Wavelet scalogram. *B*, Three most significant periodicities. *C*, Gaussian distribution of data. Note the episodic occurrence of strong ~105–330-m.yr. wavelengths. The lowermost dotted line indicates that the 30-m.yr. wavelength is significant at ~1100–1500 Ma, ~1800–2000 Ma, and ~2500 Ma but not in the Phanerozoic, where a ~27-m.yr. cyclicity is more pronounced.

A 330-m.yr. cycle occurs in most subsets over the interval 3000–1000 Ma. The absence, except very locally from the AB50-oceanic (locally a 315-m.yr. cycle) and A10 data (figs. 8, 9), may reflect the restricted age range of most AB50-oceanic and A10 data (300–0 Ma and 800–0 Ma, respectively).

A 250–220-m.yr. cycle occurs most consistently in the Late Archean–Early Proterozoic, where it is seen in all data subsets except AB50-oceanic. It also appears in most subsets between 500 Ma and the present.

A 170–160-m.yr. cycle occurs in all subsets (except AB50-oceanic). In some subsets it occurs over more limited time intervals than in others. In AB50-continental it is found between 1500 and 600 Ma (fig. 7). In the A10 analysis (fig. 9) it is present for only a short interval between about 1300 and 1000 Ma.

A 110–100-m.yr. cycle of rather short duration (2200–1400 Ma) occurs in the analysis of all data subsets, except for A10 (fig. 9) where it is conspicuously absent, perhaps replaced by a 120-m.yr. cycle between 2500–2100 Ma. In both AB50-continental and AB50-oceanic, it is weakly present at about 2200 Ma, and in AB50-continental, it is also weakly present at about 300 Ma.

There is a notable absence of cycles between about 100 and 70 m.yr. However, shorter cycles of 60, 31, 27–25, and 16–15 m.yr. are locally intense but typically only of short duration and correspond to intervals where event density is high. Analysis of AB50-continental data reveals a significant ~30-

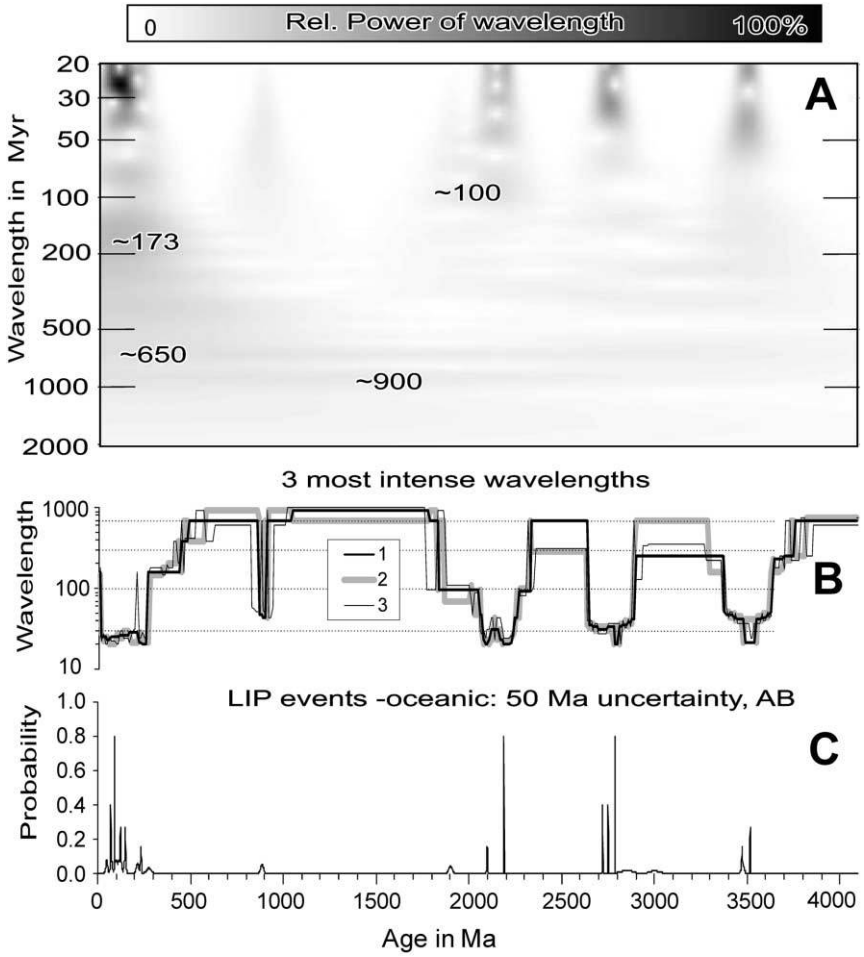

Figure 8. Wavelet analysis of AB50-oceanic data (32 events). Data described in text and listed in table 1. *A*, Wavelet scalogram. *B*, Three most significant periodicities. *C*, Gaussian distribution of data. Note that the events are clustered in the last 300 Ma.

m.yr. cycle in the ~1500–1000-Ma and ~2100–1800-Ma intervals but not during the last 300 m.yr. (fig. 7*B*). The complementary AB50-oceanic data set reveals a pronounced 27-m.yr. cycle in the last 300 m.yr. (fig. 8*B*). In the A10 data set, a significant ~27-m.yr. cycle is limited to the time interval from ~30 to 150 Ma (fig. 9*A*, 9*B*), whereas the complementary B10 analysis shows ~20–50-m.yr. cycles over scattered intervals from 2800 to 1200 Ma (fig. 10*B*).

The higher frequency 15–10-m.yr. cycle band has been assessed only for the full AB50 data set and the AB10 subset over the past 300 m.yr. (figs. 4, 6). This cycle does seem to be present and persistent in the data subset. However, its significance remains uncertain because it is rather broadband, and a 15-m.yr. cycle length is approaching the limit of age resolution for much of the data.

Summary of Wavelet Analysis. Wavelet analysis of the full data set and the various subsets (summarized in table 2) indicates that no cycles are strongly present throughout the age range of the data (3500 Ma to the present). Therefore, the data are not strongly cyclical. However, there are three weak but persistent cycles in the data that require interpretation. In addition, there are several cycles of rather short duration.

The full data set AB50 shows persistent cycles of 730–550, 330, 170–160, and perhaps 1000–900 m.yr. and cycles of shorter duration, 250–220, 105, 60, 27, and 15 m.yr. Increasing the precision of data to include only events with 2σ-age uncertainty $\leq$ 10 m.yr. (AB10) has only a minor effect.

The expression of the cycles in the various subsets reflects mostly the LIP event distribution in the subsets. For data subsets with LIP events con-

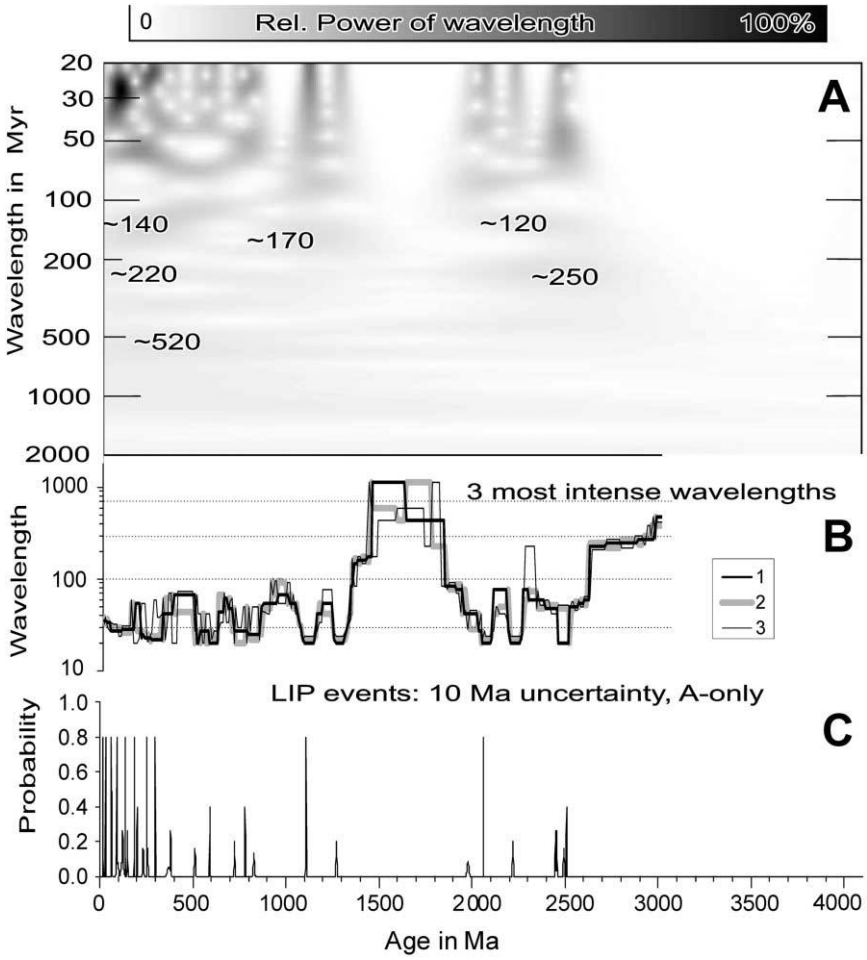

Figure 9. Wavelet analysis of A10 data (35 events). Data described in text and listed in table 1. *A*, Wavelet scalogram. *B*, Three most significant periodicities. *C*, Gaussian distribution of data. Note that the number of these events drops drastically before ~300 Ma, and they are absent before ~2500 Ma. Wavelengths of ~30 m.yr. and ~520 m.yr. are restricted to the last 150 Ma and the Phanerozoic, respectively.

centrated in the younger record, that is, AB50-oceanic and A10, only the short cycle lengths are strongly present (figs. 8, 9). In these data subsets, the 330-m.yr., 250-m.yr., and 170-m.yr. cycles are only weakly present, while the complementary AB50-continental and B10 data sets more strongly show these cycles. One exception to this pattern is that the AB50-oceanic data (fig. 8) also show weak but persistent long wavelength 650- and 900-m.yr. cycles that may correspond to the 730–550- and 1000–900-m.yr. cycles, respectively, of the other data subsets and full data set.

Spectral Analysis. We next performed spectral analysis on the data to evaluate the relative significance and variability of cycles identified by the wavelet analysis of the previous sections and also to provide a comparison between the wavelet and spectral approaches. The spectral analysis of AB50 through the last 3500 Ma shows a 705-m.yr. cycle with 99% significance above nonrandomness (fig. 11*A*). The ~320-m.yr. and ~170-m.yr. periodicities occur with greater than 95% significance. In addition, several wavelengths (44, 40, 32, 30, and 27 m.yr.) in the ~45–27-m.yr. band have greater than 90% significance. In contrast, there is no significant periodicity in the 50–150-m.yr. period band.

Most of the cycles identified by spectral (Fourier) analysis are also apparent in the wavelet analysis, for example, the 320-m.yr. and 170-m.yr. cycles. However, the 705-m.yr. cycle from the Fourier analysis corresponds to a progressively varying 730–550-m.yr. cycle observed in the wavelet analysis and points up the advantage of wavelet analysis

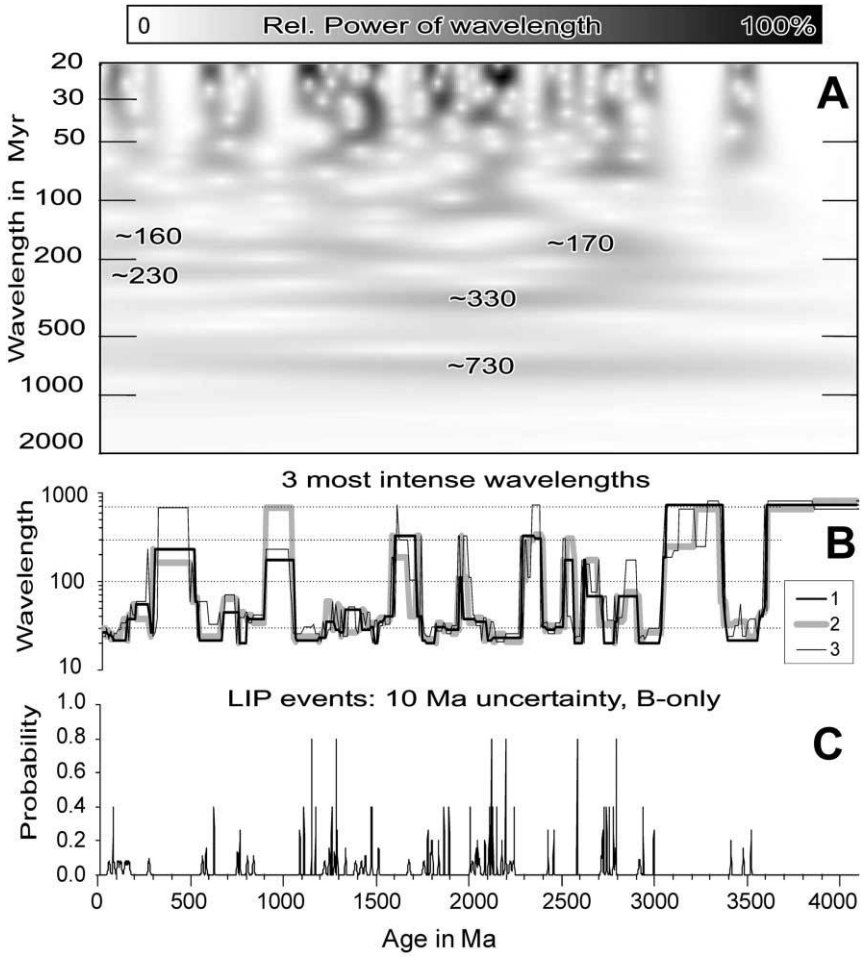

Figure 10. Wavelet analysis of B10 data (86 events). Data described in text and listed in table 1. *A*, Wavelet scalogram. *B*, Three most significant periodicities. *C*, Gaussian distribution of data. Events are common between ~1100 Ma and 3000 Ma and are clustered in three episodes ~730 Ma apart.

in recognizing progressively changing cycles. Of the numerous peaks between 45 and 27 m.yr. revealed by the Fourier analysis, only the 31- and 27-m.yr. cycles show up prominently in the wavelet analysis (where they are locally intense but only over very restricted age intervals, corresponding to higher concentrations of LIP events). The weak 900–1000-, 250–220-, and ~105-m.yr. cycles of the wavelet analysis are less significant in the Fourier analysis, confirming our earlier conclusion that they may be of limited importance.

Fourier analysis can also be used to compare data subsets with the full AB50 data set. For instance, in figure 11*B*, the AB10 Fourier spectrum shows a minor relative enhancement of ~170-m.yr. and ~27-m.yr. cycles and diminishment of ~320-m.yr. and 30–40-m.yr. cycles in comparison with the Fourier spectrum of the full AB50 data set. This observation suggests that the cycles are only weakly affected by varying the age uncertainty criteria; this has been previously noted in the wavelet analysis.

In figure 12, we focus on the last 850 m.yr., which has a higher frequency of LIP events and more precise ages than the pre-850-Ma period. The full data set AB50 and subsets AB10 and B10 show a continuum of frequencies of similar magnitude. Only subset A10 shows any preferred cycles, of magnitude 27, 15, and 12 m.yr. We conclude that cycles of <70 m.yr. are of uncertain significance, a conclusion also reached from the wavelet analysis.

Cross-Spectral Analysis of Data Subsets. Cross-spectral analysis provides an opportunity to assess the correlation or lack of correlation between different subsets of the data. A dramatic lack of correlation is exhibited by the comparison of A10 and B10 data. Cross-spectral analysis shows that the

Table 2. Summary of Cycles and Their Durations Identified Using Wavelet Analysis

Cycle lengths (m.yr.)	AB50 (full data set; $n = 154$; figs. 3, 4; Ga)	AB10 (precisely dated subset; $n = 120$; figs. 5, 6; Ga)	A10 (plume-linked subset; $n = 35$; Ga)	B10 (probably plume-linked subset; $n = 86$; Ga)	AB50-continental (continental LIP subset; $n = 115$; fig. 7; Ga)	AB50-oceanic (oceanic LIP subset; $n = 32$; fig. 8; Ga)
1000–900	2.0–0[a]	weak 2.0–0[a]	…	…	…	2.0–0[a]
730–550	3.3–0[a]	2.6–0[a]	.7–0	3.5–.6	…	weak 2.5–0
330	3.0–1.0	2.9–1.0	…	2.9–1.1	2.6–1.5	…
250–220	3.3–2.1; .7–0	3.0–2.2; .8–.1	2.5–2.1; ~.2	3.0–2.5; 1.1–.1	2.8–2.4	…
170–160	~2.7; 1.6–0	2.8–2.5; 1.7–0	1.3–1.0	2.9–2.4; 1.5–1.1	1.5–.6	…
105	2.2–1.4	2.2–1.7	2.5–2.1 (120-m.yr. cycle)	2.2–1.7	2.2–1.5; ~.4 (110-m.yr. cycle)	~2.2
<70 (notably, ca. 60, 30, and 15)[b]	Locally intense over limited intervals	Locally intense over limited intervals	…	Locally intense over limited intervals	Locally intense over limited intervals	Locally intense over limited intervals

[a] Cycle length shows progressive or steplike decrease from 730 to 550 m.yr. over the interval 3500 Ma to present. The still weaker 900–1000-m.yr. cycle appears and increases from 900 to 1000 m.yr. over the interval 2000 Ma to present. At about 2000 Ma, the 730–550- and 1000–900-m.yr. cycles converge.
[b] Only past 300 m.yr. considered to have enough precisely dated large igneous provinces to assess cycles of this wavelength range.

periodicity of the A10 and B10 LIP events (over the last 850 m.yr.) are significantly out of phase over the full range of wavelengths (fig. 13). This is similar to the result from the wavelet analysis, which indicated that A and B LIP data show different cycle patterns.

Strong discordance is also observed between the complementary AB50-continental and AB50-oceanic data subsets over the period 300 Ma to the present (fig. 14). The AB50-continental data show numerous peak cycles (60, 33, 23, and 16 m.yr.), but there is only one important peak in the AB50-oceanic data, at 27 m.yr. These two data subsets are strongly out of phase for most of the past 300 Ma, and thus it can be inferred that the two data subsets do not correlate. This conclusion is robust since both data sets are densely populated over this time interval.

Summary of Spectral and Cross-Spectral Analyses. Spectral analysis sheds light on the significance of cycles observed in the wavelet analyses, and cross-spectral analysis contributes to the understanding of the comparison between data subsets. In particular, the potential importance of the cycles of 730–550 (or 705), 320, 170, and 27 m.yr. is reinforced, whereas the 250- and 105-m.yr. cycles appear to be less robust. The A10 and B10 data subsets are shown to be uncorrelated over the past 850 m.yr., as are the oceanic (AB50-oceanic) and continental (AB50-continental) subsets, especially during the past 300 m.yr.

Timing of Cycle-Peaks. An additional type of cross-spectral analysis was carried out in order to determine the timing of the peaks in the relatively prominent 170-m.yr. cycle and in the 27-m.yr. cycle (one of the more important shorter-wavelength cycles). Cross-spectral analysis of the AB50 time series with sinusoidal 170-m.yr. and 27-m.yr. cycles of amplitude 1 through the last 1500 Ma is used to calculate the optimal phase shift between data and periodicity for modeling purposes (fig. 15). The phase shift of the 170-m.yr. cycle is −2.83 radians, indicating that the most recent maximum occurs at 76.5 Ma. The 27-m.yr. cycle is 0.83 radians phase shifted, which means that the most recent maximum occurs at $27 - 3.6$ Ma $= 23.4$ Ma.

Figure 16*A* shows the fit of the model $x(t) = \cos(2\pi t/170 - 77$ m.yr.) to the LIP data where time t is in m.yr. Through the last 1500 Ma, seven of nine peaks in the 170-m.yr. cycle model correspond roughly to clusters of LIP events, including the significant 90–60-m.yr. period of global LIP activity and the 250-Ma Siberian flood basalt event. Completely missing are event clusters at ~420 Ma and ~950 Ma. In addition, during the past 300 m.yr. LIP events occur not only at the 170-m.yr. peaks but also between peaks, likely reflecting the presence of other cycles as observed in the wavelet analysis. Overall, between 1500 and 500 Ma there is moderate correlation with the 170-m.yr. cycle. However, prior to 1500 Ma, about 50% of the peaks in the 170-m.yr. cycle model lack corresponding LIP events.

The cause of this discrepancy is unclear. It could indicate that the pre-1500-Ma events do not conform to a 170-m.yr. cycle. However, prominent events between 2800 and 2700 Ma yield a 170-m.yr. cyclicity in the wavelet analysis (e.g., see fig. 3). This suggests either (1) that the 170-m.yr. wave-

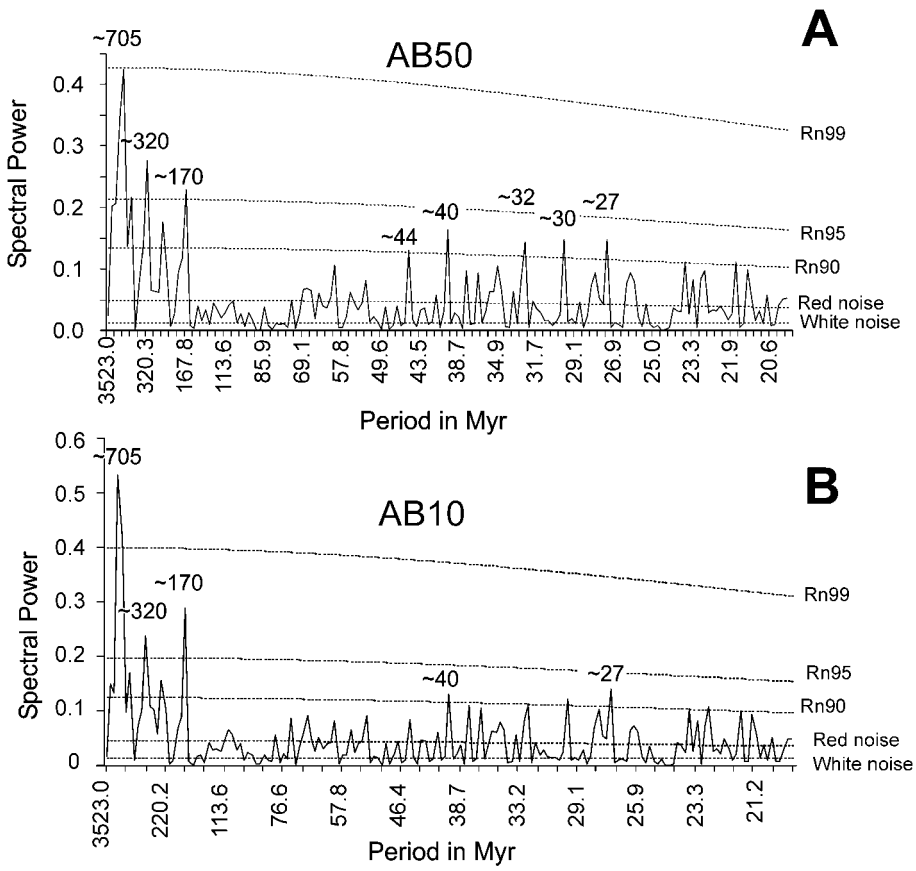

Figure 11. Spectral analysis of AB50 and AB10 events in the last 3500 Ma, including white and red noise and Rn_{99}, Rn_{95}, and Rn_{90} significance calculations (see text for explanation). Note that ~27-m.yr. and ~170-m.yr. cycles are enhanced in the higher precision AB10 data set.

length used in the analysis of the figure 16*A* is only approximately incorrect and leads to an accumulated offset over many cycles or (2) that there is a discontinuity in the LIP event pattern in the 170-m.yr. cyclicity for 2800–2700 Ma and 1500 Ma–present.

The 27-m.yr. cyclicity model $x(t) = \cos(2\pi t/27 + 3.6$ m.yr.) shows poor graphical correlation with the events in the last 300 Ma (fig. 16*B*), in particular with events that can be explained by ~170-m.yr. cycle (e.g., Paleogene/Late Cretaceous). In some time intervals, however (e.g., ~1950–2350 Ma in fig. 16*C*), the fit is better. Because the 27-m.yr. cycle is not an even multiple of 170 m.yr., it cannot be an integrated part of the 170-m.yr. cycle and must be of independent origin.

Discussion

Origin of Cycles. The wavelet and Fourier (spectral) analysis of the previous sections indicate that the LIP flux is relatively continuous through time. However, within this rather constant distribution of LIP events, several semipersistent weak cycles are observed.

~170-m.yr. Cycle. Both wavelet and spectral analysis reveal a ~170-m.yr. cycle that is significant at the >95% confidence level (fig. 11) and that is present with varying strength over major time intervals (figs. 3, 5, 7, 10; table 2). Seven of nine cycle peaks are represented by A10 events (fig. 16*A*). The last maximum in this cycle occurred at ~77 Ma and covers the Cenomanian to Early Paleogene events. However, in comparison with the actual event record (fig. 16*A*), the correlation is with clusters of LIP events rather than individual LIPs. For instance, the first peak at 77 Ma represents the average of extensive LIP activity at 65–60 Ma (Deccan and North Atlantic Igneous Province) and at 90 Ma (second pulse of Ontong Java, Caribbean/Columbian, and Queen Elizabeth Islands–Alpha Ridge, and Madagascar LIPs).

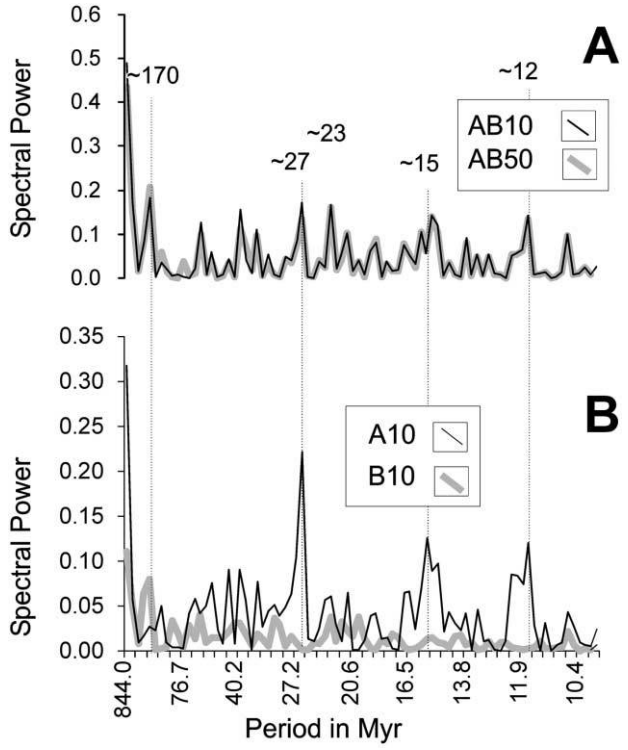

Figure 12. Detailed spectral analysis for the last 844 Ma. Note that the ~27-m.yr., 15-m.yr., and ~12-m.yr. periodicities remain unchanged with decreasing level of age uncertainty (AB10 to AB50) but decrease with decreasing confidence in a plume link (A10 to B10).

So our preliminary conclusion is that the 170-m.yr. cycle may correspond to clusters of LIP events, which can also be termed superplume events (Condie 2001; Ernst and Buchan 2002). However, it should be noted that the classic superplume event of Larson (1991) that starts with Ontong Java and Manihiki Plateaus at 122 Ma does not match any peak in the 170-m.yr. cycle.

730–550-m.yr. Cycle. The 730–550-m.yr. cycle is of weak intensity but long duration in the wavelet analysis of the full AB50 data set and is present in most subsets including the sparse AB50-oceanic data. It also corresponds to the 705-m.yr. cycle in the Fourier analysis. By its duration, we may speculate that it has a link with a supercontinent cycle (e.g., Nance et al. 1988; Condie 2002). The presence in the AB50-continental record would suggest a link with supercontinent breakup (representing bursts of breakup related LIPs). The weaker presence of a 650-m.yr. cycle in the oceanic record might indicate a link with bursts of production of oceanic plateaus or enhanced preservation of oceanic LIPs during supercontinent formation (e.g., Condie 2001, 2002). Isley and Abbott (2002) have linked their similar length 800-m.yr. cycle to core nutations. An alternative hypothesis is that the 730–550-m.yr. (650-m.yr.) cycle is a multiple of the 170-m.yr. cycle, in which case the 170-m.yr. cycle would be fundamental. The longer wavelengths would occur because of intervals in which 170-m.yr. cycle events are absent. The weak 1000–900-m.yr. cycle is of uncertain significance.

<70-m.yr. Cycles. Cycles <70 m.yr. are characterized by their persistence over only short intervals, according to the wavelet analysis, and sometimes represent a near continuum of frequencies. The most intense (but intermittent) cycles are those with peaks at 27 and 15 m.yr.

Comparison of Complementary Subsets of the LIP Database

A- versus B-Rated Data. Both wavelet and spectral analyses demonstrate that the A and B data are strongly uncorrelated. There are two possible interpretations: A and B data represent distinct classes of LIPs, or the differences relate to the higher concentration of A data in the young record.

The differences between A and B data mainly represent differences in the confidence regarding the size and duration of events, with the events rated A having stronger evidence for a large-volume, short-duration event and hence having a stronger link to a plume. So as the database im-

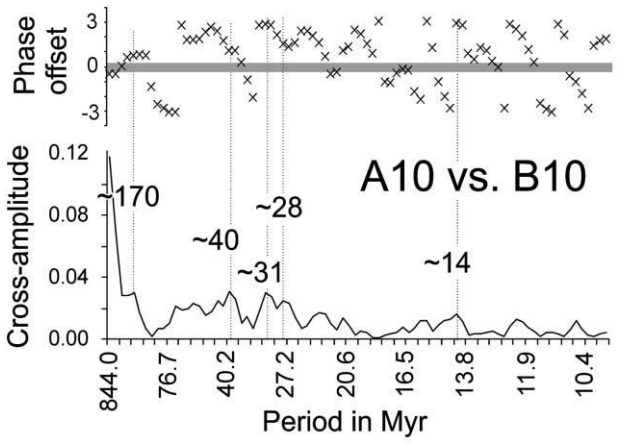

Figure 13. Cross-spectral analysis of large igneous provinces for the last 844 Ma: pairs of cross-amplitude and phase spectra for A10 versus B10. Vertical lines mark high cross-spectral amplitudes. Thick gray line marks "in phase" band (i.e., periodic fluctuations linearly correlated with <5% off-set). Note that major periodic fluctuation in A10 and B10 are out of phase. Phase offset is in radians.

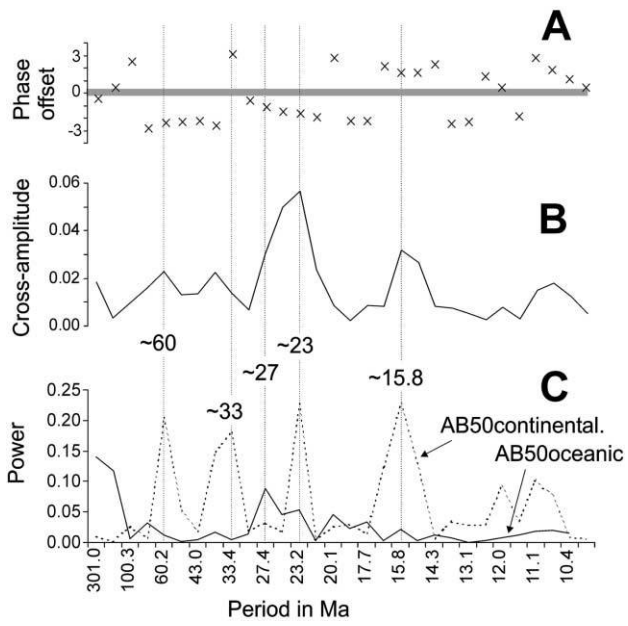

Figure 14. Spectral (*C*) and cross-spectral (*A* and *B*) analysis of AB50-continental data (*dotted line*) with AB50-oceanic data (*solid line*) during the last 300 Ma. Note that ~27-m.yr. cycle is significant only in the AB50-oceanic data set while ~15.8-, 23-, 33-, and 60-m.yr. cyclicities are evident only in the continental data set. Also note that none of the major periods are in-phase.

proves, many B events will probably be converted into A events. In addition, there are also categorical differences between A and B data requiring assessment. For instance, A data include events with giant radiating dike swarms while B data include events with giant linear swarms, mainly distributed throughout the Proterozoic. Perhaps this difference represents independent populations of LIPs, that is, a plume setting for radiating swarms and a rift or back-arc setting for linear swarms. However, improved mapping and dating in the past has resulted in some giant linear swarms being assembled into giant radiating swarms (Ernst and Buchan 1997). Another categorical difference between A and B data is inclusion of Archean greenstone belts containing komatiites in the B set. However, high Mg rocks (mainly picrites) may also be present in A events of Phanerozoic age. We have retained the B classification for Archean greenstone belts containing komatiites until more consensus is obtained on their geodynamic setting.

Oceanic versus Continental LIP Record. Spectral analysis indicates a significant mismatch between the cycle patterns associated with oceanic and continental LIP data subsets for the past 300 m.yr. (fig. 14). Whether this mismatch extends to the entire record must await a more robust oceanic LIP record.

Comparison with Cycles Identified in Previous Time-Series Analyses. The cycles identified in previous analyses of LIP data were summarized in the "Introduction." The weak cycles that we observe in this article are only broadly similar to those previous results. The 500–300-m.yr. cycle of Yale and Carpenter (1998) may be present as our Proterozoic 330-m.yr. cycle. Examining the Isley and Abbott (2002) time-series analysis of high Mg rocks, we do not see their 273 $\pm$ ~20-m.yr. cycle, which they link with a galactic year, nor their 819 + 204/−137-m.yr. cycle, which they link with core nutations. However, given the bandwidth uncertainties, it remains possible that their 273-m.yr. cycle is the same as our 250–220 Ma, and their 800-m.yr. cycle would correspond to our 730–550-m.yr. cycle (or our faint 1000–900-m.yr. cycle). Their less significant periodicity of 315 $\pm$ 25 m.yr. may correspond to our 330-m.yr. periodicity, but their 372 $\pm$ 35-m.yr. cycle is not present in our data. While we observed cycles in the 25–35 m.yr. range in the last 300 Ma, wavelet analysis reveals that they are not persistent through Earth's history. This is probably

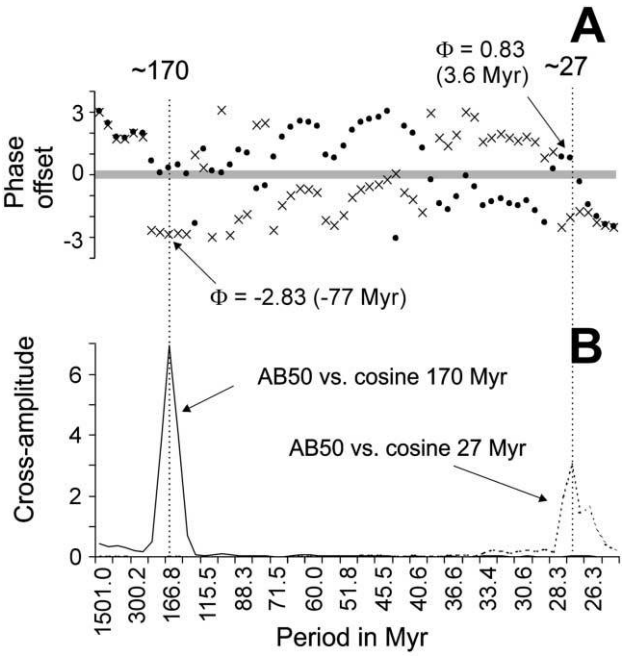

Figure 15. Cross-spectral analysis of AB50 data with potential periodicity (27 and 170 m.yr.) over the last 1500 Ma. *A*, Phase offsets (in radians) of AB50 versus 170 m.yr. identified by dots, and phase offset of AB50 versus 27 m.yr. identified by x's. *B*, Cross-amplitudes.

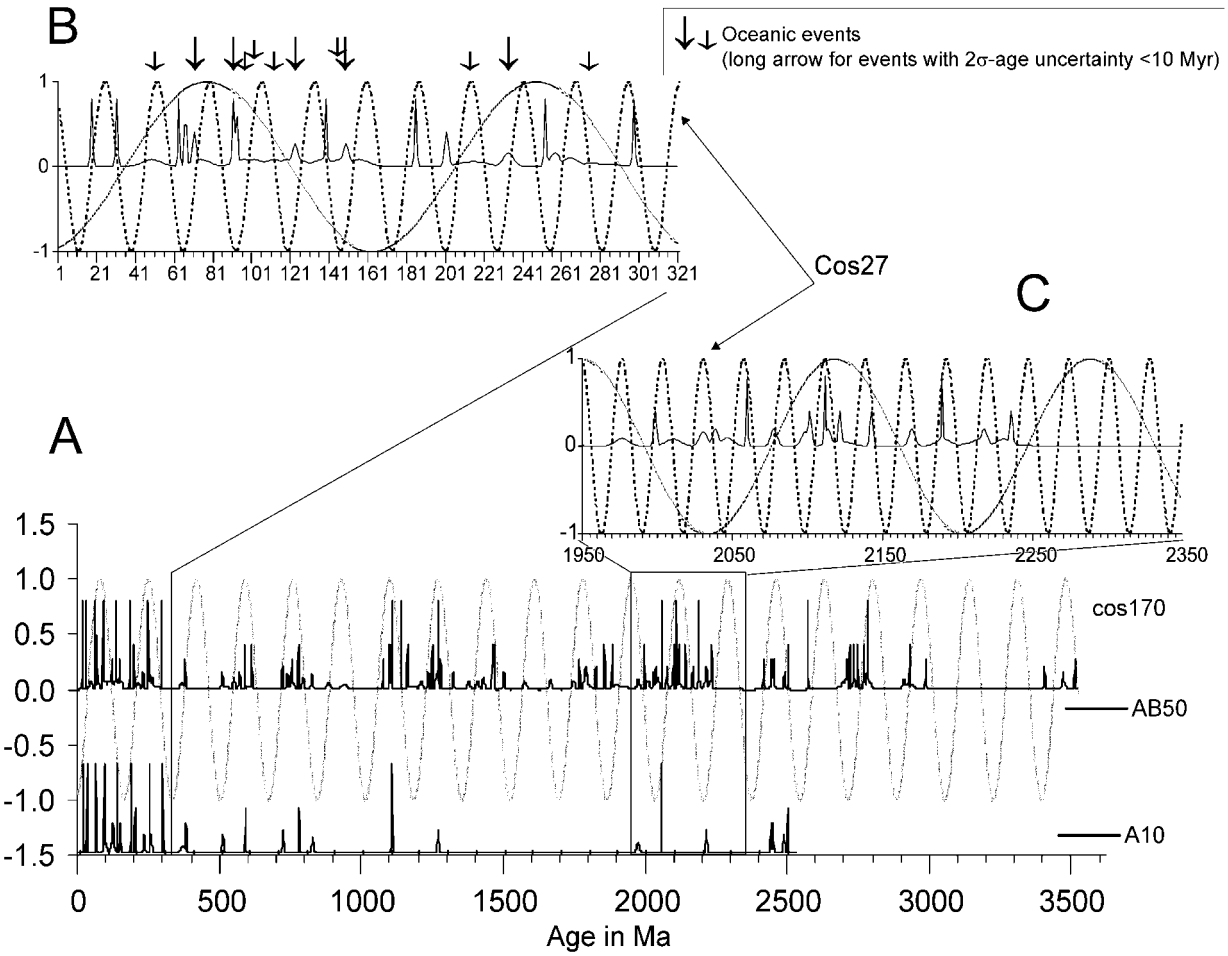

Figure 16. Comparison of AB50 data and A10 data with a 170-cosinusoidal model (phase-shift = −77 Ma; see fig. 13). *A*, Last 3500 Ma. *B*, Zoom-in for last 320 Ma with +3.6 Ma phase-shifted 27-m.yr. cycle (*dotted line*). *C*, Time interval from 1950–2350 Ma with zero phase shift. Note that the 27-m.yr. cycle cannot be graphically correlated with large igneous province events during the last 320 Ma but does correlate with 14 of 20 events during 1950–2350 Ma.

because the high density of LIPs required for the identification of cycles of such short wavelength is present only in a few restricted intervals. The 17 ± 1.5-m.yr. minor cycle of Isley and Abbott (2002; fig. 2) is not present in our data, but the 15.4-m.yr. cycle length calculated by Rampino and Caldeira (1993) is locally prominent in our data. It is also interesting that the Isley and Abbott (2002) study does not observe one of our strongest cycles, 170 m.yr.

We performed an additional test to assess the origin of the difference between our results and those of Isley and Abbott (2002). All of our analyses were done using the OR approach to summing Gaussian curves, while Isley and Abbott (2002) used the AND approach. Therefore, we performed an additional wavelet analysis on our AB50 data using their AND approach (fig. 17). The resulting wavelet pattern using AND is very similar to the result using the OR approach (cf. figs. 3, 17); the relative power and location of significant wavelengths remain the same (maximum 8% difference in wavelength and no change in location). While the differences between both figures 3 and 17 are small, we should note that the differences between AND and OR approaches would probably be greater for data sets containing a large number of adjacent events with large age uncertainties and therefore significant overlaps in the computed Gaussian age distributions.

The comparison of figures 3 and 17 basically confirms that the difference between our analysis and the analysis of Isley and Abbott (2002) is not primarily a function of technique but is more strongly a consequence of the differences between the LIP

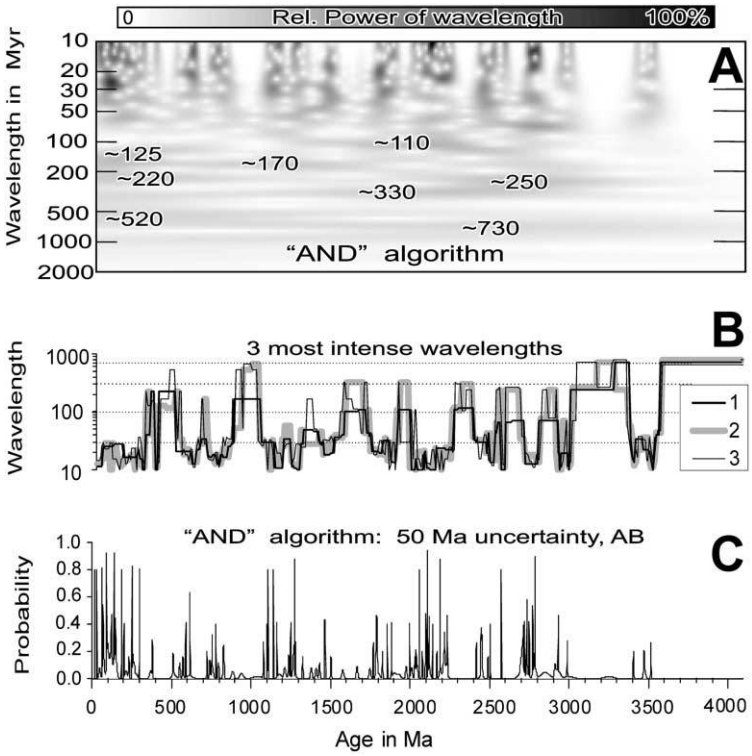

Figure 17. Analysis of AB50 data converted to continuous spectrum using AND approach for comparison with figure 3, which shows the same data set converted to continuous data using OR approach. AND and OR analysis described in the text.

database we have used and that used by Isley and Abbott (2002). While they focused on LIPs identified by high Mg sequences, we attempted to include a broader population of LIPs. Continuing research on mafic magmatism, particularly using high-precision dating, will lead to a significant improvement in the LIP database over the next decade. It will probably require a few more iterations of time-series analyses on this improving LIP database before we can be confident that the weak cycles that we recognize in this article are real.

Comparison with Earth System Cycles. Some of the most continuous of Earth system cycles are expressed in seawater isotopic compositions recorded by marine carbonates (Veizer et al. 1999). The recently published Bochum/Ottawa Isotopic Data Set is a dramatic improvement in the consistency of the Phanerozoic data and was analyzed using wavelet analysis. In this database, Prokoph and Veizer (1999) identify a strong 94-m.yr. cycle in Sr isotopes, a 100-m.yr. cycle in C isotopes, and a 125-m.yr. cycle in O isotopes. However, this dramatic 94–125-m.yr. cyclicity in the Phanerozoic seawater record seems to be only weakly expressed in our data. This could be interpreted to indicate that LIPs are not a strong control on the 94–125-m.yr. cyclicity of oceanic seawater composition. However, a direct comparison of LIP and oceanic seawater data sets is required to fully test this notion.

Shorter cycles are also observed in the sedimentary record, and their link with LIPs remains to be tested. A ~30-m.yr. periodicity in the seawater chemistry, in particular strontium, carbon, and oxygen isotope composition (Prokoph and Veizer 1999), may be at least partially related to the release of greenhouse gases from LIP events (e.g., Stothers 1993). A 15-m.yr. cycle is also observed in the high-resolution fossil record (e.g., planktonic foraminifera and nannoplankton; A. Prokoph, unpublished data).

As noted earlier, the weak but persistent 730–550- (650)-m.yr. cycle may be linked with a supercontinent or core nutation cycle, and the 170 m.yr. cycle may be linked to clusters of LIP events. The 330-m.yr. cycles cannot yet be explained, although there is the intriguing possibility that the 170-m.yr. cycle is fundamental and that the 330-m.yr. (and perhaps 650-m.yr.) cycles are simply multiples. In this case, intervals of absent events ("miss-

ing" data) could produce the longer cycles. It is also possible that the opposite is true: that the 650-m.yr. cycle is fundamental, and the 170- and 330-m.yr. cycles are harmonics, because a very "spiky" pattern of events will be Fourier transformed into a set of sinusoidal fluctuating spectral values with a spacing of frequency f (original spacing between events), $2f$, $4f$ (e.g., Davis 1986) or, alternatively, wavelengths p, $p/2$, $p/4$. However, the fundamental nature of the ~170-m.yr. interval spacing is supported by the association with clusters of LIP events over the last 1500 Ma (fig. 16).

Future Work. As the database of LIPs improves, future time-series analyses will reveal which of the cycles we observe are enduring and/or which are a function of an incomplete database. An improved database should allow the data to be subdivided into more statistically robust subsets in order to identify any independent overlapping cycles related to LIPs of different origins (e.g., plume and nonplume) and settings (e.g., continental and oceanic). The approach laid out here is a template for such future analyses. In addition, joint analysis of LIPs with other kinds of databases such as seawater isotopic composition needs to be performed in order to better understand the origin of the cycles of 25–35 m.yr., 170 m.yr., 330 m.yr., and 730–550 m.yr. that we have observed in the LIP data.

ACKNOWLEDGMENTS

This is Geological Survey of Canada publication 2003068. We appreciate the extremely detailed and helpful comments by A. Isley, F. Agterberg, and an anonymous reviewer.

REFERENCES CITED

Bleeker, W. 2002. Archaean tectonics: a review, with illustrations from the Slave craton. *In* Fowler, C. M. R.; Ebinger, C. J.; and Hawkesworth, C. J., eds. The early earth: physical, chemical and biological development. Geol. Soc. Spec. Publ., Geol. Soc. Lond. 199:151–181.

Buchan, K. L., and Ernst, R. E. 2004. Diabase dike swarms and related units in Canada and adjacent regions. Geol. Surv. Can., map 2022A (with report), scale 1 : 5,000,000.

Buchan, K. L.; Hodych, J. P.; Roddick, J. C.; Emslie, R. F.; and Hamilton, M. A. 1996. Paleomagnetism and U-Pb geochronology of Mesoproterozoic dykes of Labrador and correlations with dykes of southwest Greenland. *In* Proterozoic Evolution of the North Atlantic Realm (Program and Abstracts) Conference (Goose Bay, Labrador, Canada), p. 37.

Campbell, I. H. 2001. Identification of ancient mantle plumes. *In* Ernst, R. E., and Buchan, K. L., eds. Mantle plumes: their identification through time. Geol. Soc. Am. Spec. Pap. 352:1–21.

Chao, B. F., and Naito, I. 1995. Wavelet analysis provides a new tool for studying Earth's rotation. EOS: Trans. Am. Geophys. Union 76:161, 164–165.

Coffin, M. F., and Eldholm O. 1994. Large igneous provinces: crustal structure, dimensions, and external consequences. Rev. Geophys. 32:1–36.

———. 2001. Large igneous provinces: progenitors of some ophiolites? *In* Ernst, R. E., and Buchan, K. L., eds. Mantle plumes: their identification through time. Geol. Soc. Am. Spec. Pap. 352:59–70.

Coffin, M. F.; Pringle, M. S.; Duncan, R. A.; Gladczenko, T. P.; Storey, M.; Müller, R. D.; and Gahagan, L. A. 2002. Kerguelen hotspot magma output since 130 Ma. J. Petrol. 43:1121–1139.

Condie, K. C. 2001. Mantle plumes and their record in earth history. Cambridge, Cambridge University Press, 306 p.

———. 2002. The supercontinent cycle: are there two patterns of cyclicity? J. Afr. Earth Sci. 35:179–183.

Courtillot, V.; Jaupart, C.; Manighetti, I.; Tapponnier, P; and Besse, J. 1999. On causal links between flood basalts and continental breakup. Earth Planet. Sci. Lett. 166:177–195.

Davis, J. C. 1986. Statistics and data analysis in geology. New York, Wiley, 646 p.

Deblond, A.; Punzalan, L. E.; Boven, A.; and Tack, L. 2001. The Malagarazi Supergroup of southeast Burundi and its correlative Bukoba Supergroup of northwest Tanzania: Neo– and Mesoproterozoic chronostratigraphic constraints from Ar-Ar ages on mafic intrusive rocks. J. Afr. Earth Sci. 32:435–449.

Duncan, R. A. 2002. A time frame for construction of the Kerguelen Plateau and Broken Ridge. J. Petrol. 43: 1109–1119.

Eriksson, P. G.; Condie, K. C.; van der Westhuizen, W.; van der Merwe, R.; de Bruiyn, H.; Nelson, D. R.; Altermann, W.; et al. 2002. Late Archaean superplume events: a Kaapvaal-Pilbara perspective. J. Geodynam. 34:207–247.

Ernst, R. E., and Buchan, K. L. 1997. Giant radiating dyke swarms: their use in identifying pre-Mesozoic large igneous provinces and mantle plumes. *In* Mahoney, J. J., and Coffin, M. F., eds. Large igneous provinces: continental, oceanic and planetary flood volcanism. Am. Geophys. Union Geophys. Monogr. 100:297–333.

———. 2001*a*. Large mafic magmatic events through time and links to mantle plume heads. *In* Ernst, R. E., and Buchan, K. L., eds. Mantle plumes: their identification through time. Geol. Soc. Am. Spec. Pap. 352: 483–575.

———, eds. 2001*b*. Mantle plumes: their identification through time. Geol. Soc. Am. Spec. Pap. 352, 593 p.
———. 2002. Maximum size and distribution in time and space of mantle plumes: evidence from large igneous provinces. *In* Condie, K. C.; Abbott, D.; and Des Marais, D. J., eds. Superplumes in time and space. J. Geodynam. Spec. Issue. 34:309–342; erratum, 34:711–714.
———. 2003. Recognizing mantle plumes in the geological record. Annu. Rev. Earth Planet. Sci. 31:469–523.
Ernst, R. E.; Buchan, K. L.; and Prokoph, A. 2003. Large igneous province record through time. *In* Eriksson, P. G.; Altermann, W.; Nelson, D. R.; Mueller, W. U.; and Catuneanu, O., eds. The Precambrian Earth: tempos and events. Amsterdam, Elsevier, in press.
Ernst, R. E.; Buchan, K. L.; West, T. D; and Palmer, H. C. 1996. Diabase (dolerite) dyke swarms of the world (1st ed.). Geol. Surv. Can., Open File 3241, includes map, scale 1 : 35,000,000 at equator and report, 104 p.
Hamilton, M. A.; Davis, D. W.; Buchan, K. L.; and Halls, H. C. 2002. Precise U-Pb dating of reversely magnetized Marathon diabase dykes and implications for emplacement of giant dyke swarms along the southern margin of the Superior Province, Ontario. Radiogenic age and isotopic studies, report 15, Geol. Surv. Can. Curr. Res. 2002-F6, 8 p.
Isley, A. E., and Abbott, D. H. 1999. Plume-related mafic volcanism and the deposition of banded iron formation. J. Geophys. Res. 104:15,461–15,478.
———. 2002. Implications for the temporal distribution of high-Mg magmas for mantle plume volcanism through time. J. Geol. 110:141–158.
King, S. D., and Anderson, D. L. 1998. Edge-driven convection. Earth Planet. Sci. Lett. 160:289–296.
Larson, R. L. 1991. Latest pulse of Earth: evidence for a mid-Cretaceous superplume. Geology 19:547–550.
———. 1997. Superplumes and ridge interactions between Ontong Java and Manihiki plateaus and the Nova-Canton trough. Geology 25:779–782.
Li, Z. X.; Li, X. H.; Kinny, P. D.; Wang, J.; Zhang, S.; and Zhou, H. 2003. Geochronology of Neoproterozoic synrift magmatism in the Yangtze Craton, South China and correlations with other continents: evidence for a mantle superplume that broke up Rodinia. Precambrian Res. 122:85–109.
Mann, M. S., and Lees, J. M. 1996. Robust estimation of background noise and signal detection in climatic time series. Clim. Change 33:409–445.
Moores, E. M. 2002. Ophiolites and plumes in Earth history, their tectonic and environmental implications. Superplume International Workshop, Tokyo, January 28–31, 2002 (abstract volume), Tokyo Institute of Technology.
Nance, R. D.; Worsley, T. R.; and Moody, J. B. 1988. The supercontinent cycle. Sci. Am. 259:44–52.
Nikishin, A. M.; Ziegler, P. A.; Abbott, D.; Brunet, M.-F.; and Cloetingh, S. 2002. Permo-Triassic intraplate magmatism and rifting in Eurasia: implications for mantle plumes and mantle dynamics. Tectonophysics 351:3–39.
Oberthür, T.; Davis, D. W.; Blenkinsop, T. G.; and Höhndorf, A. 2002. Precise U-Pb mineral ages, Rb-Sr and Sm-Nd systematics for the Great Dyke, Zimbabwe: constraints on late Archean events in the Zimbabwe craton and Limpopo belt. Precambrian Res. 113:293–305.
Park, J., and Maasch, K. A. 1993. Plio-Pleistocene time evolution of the 100-kyr cycle in the marine paleoclimate records. J. Geophys. Res. 98:447–463.
Peate, D. W. 1997. The Paraná-Etendeka Province. *In* Mahoney, J. J., and Coffin, M. F., eds. Large igneous provinces: continental, oceanic, and planetary flood volcanism. Am. Geophys. Union Geophys. Monogr. 100: 217–245.
Pirajno, F.; Morris, P. A.; and Wingate, M. T. D. 2002. A possible large igneous province (LIP) in central Western Australia: implications for mineralisation models. Australian Geological Convention, 16th (Adelaide, Australia, July 2002).
Prokoph, A., and Barthelmes, F. 1996. Detection of nonstationarities in geological time series: wavelet transform of chaotic and cyclic sequences. Comput. Geosci. 22:1097–1108.
Prokoph, A., and Veizer, J. 1999. Trends, cycles and nonstationarities in isotope signals of Phanerozoic seawater. Chem. Geol. 161:225–240.
Rampino, M. R., and Caldeira, K. 1993. Major episodes of geologic change: correlations, time structure and possible causes. Earth Planet. Sci. Lett. 114:215–227.
Reichow, M. K.; Saunders, A. D.; White, R. V.; Pringle, M. S.; Al-Mukhamedov, A. I.; Medvedev, A. I.; and Kirda, N P. 2002. $^{40}Ar/^{39}Ar$ dates from the West Siberian Basin: Siberian flood basalt province doubled. Science 296:1846–1849.
Saunders, A. D.; Fitton, J. G.; Kerr, A. C.; Norry, M. J.; and Kent, R. W. 1997. The North Atlantic igneous province. *In* Mahoney, J. J., and Coffin, M. F., eds. Large igneous provinces: continental, oceanic, and planetary flood volcanism. Am. Geophys. Union Geophys. Monogr. 100:45–93.
Stern, R. A.; Machado, N.; Syme, E. C.; Lucas, S. B.; and David, J. 1999. Chronology of crustal growth and recycling in the Paleoproterozoic Amisk collage (Flin Flon Belt), Trans-Hudson Orogen, Canada. Can. J. Earth Sci. 36:1807–1827.
Storey, B. C. 1995. The role of mantle plumes in continental breakup: case histories from Gondwanaland. Nature 377:301–308.
Stothers, R. B. 1993. Flood basalts and extinction events. Geophys. Res. Lett. 20:1399–1402.
Teixeira, W.; Sabaté, P.; Barbosa, J.; Noce, C. M.; and Carneiro, M. A. 2000. Archean and Paleoproterozoic tectonic evolution of the São Francisco craton, Brazil. *In* Cordani, U. G.; Milani, E. J.; Thomaz Filho, A.; and Campos, D. A., eds. Tectonic evolution of South America. Int. Geol. Cong., 31st Brazil 2000 (Rio De Janeiro, 2000), p. 101–137.
Tolan, T. L.; Reidel, S. P.; Beeson, M. H.; Anderson, J. L.; Fecht, K. R.; and Swanson, D. A. 1989. Revisions to the estimates of the areal extent and volume of the

Columbia River Basalt Group. *In* Reidel, S. P., and Hooper, P. R., eds. Volcanism and tectonism in the Columbia River flood-basalt province. Boulder, Colo., Geol. Soc. Am. Spec. Pap. 239:1–20.

Tomlinson, K. Y., and Condie, K. C. 2001. Archean mantle plumes: evidence from greenstone belt geochemistry. *In* Ernst, R. E., and Buchan, K. L., eds. Mantle plumes: their identification through time. Geol. Soc. Am. Spec. Pap. 352:341–357.

Torsvik, T. H.; Tucker, R. D.; Ashwal, L. D.; Eide, E. A.; Rakotosolofo, N. A.; and de Wit, M. J. 1998. Late Cretaceous magmatism in Madagascar: palaeomagnetic evidence for a stationary Marion hotspot. Earth Planet. Sci. Lett. 164:221–232.

Veizer, J. 1988. The evolving exogenic cycle. *In* Gregor, C. B.; Garrels, R. M.; Mackenzie, F. T.; and Maynard, J. B., eds. Chemical cycles in the evolution of the earth. New York, Wiley, p. 175–220.

Veizer, J.; Ala, D.; Azmy, K.; Bruckschen, P.; Buhl, D.; Bruhn, F.; Carden, G. A. F.; et al. 1999. $^{87}Sr/^{86}Sr$, $\delta^{13}C$ and $\delta^{18}O$ evolution of Phanerozoic seawater. Chem. Geol. 161:59–88.

White, R. S., and McKenzie, D. P. 1989. Magmatism at rift zones: the generation of volcanic continental margins and flood basalts. J. Geophys. Res. 94:7685–7729.

Wingate, M. T. D.; Pisarevsky, S. A.; and Evans, D. A. D. 2002. Rodinia connections between Australia and Laurentia: no SWEAT, no AUSWUS? Terra Nova 14: 121–128.

Yale, L. B., and Carpenter, S. J. 1998. Large igneous provinces and giant dike swarms: proxies for supercontinent cyclicity and mantle convection. Earth Planet. Sci. Lett. 163:109–122.